Supplementary Information for

Title: Multilayered mechanisms ensure that short chromosomes recombine in meiosis

This PDF file includes:

Supplementary Discussion

1, A hypothesis: distinct early and late mechanisms govern DSB protein behavior

It remains unresolved why negative feedback tied to homolog engagement affects chromosomes differently in relation to their size. One hypothesis, supported by lifespans of resected DSBs[44], is that smaller chromosomes tend to terminate DSB formation later because they take longer on average to find their homologous partners[2,16]. Perhaps the time necessary for finding the homolog is determined by the total number (not density) of DSBs and recombination events per chromosome, with the total number primarily determined by the size[12,15]. (A different, nonexclusive mechanism involving special behaviors of domains near chromosome ends is discussed below in section 5.)

How homolog engagement inhibits DSB formation is likewise not known. However, studies in yeast and mice revealed that pro-DSB factors including Rec114 and Mer2 are preferentially bound to chromosome segments that have not synapsed with a partner[3,7,8,10,57], and that formation of synaptonemal complex provokes active displacement of these proteins[7,10,19].

Putting these ideas together, a straightforward hypothesis is that feedback from homolog engagement is sufficient to explain all of the negative correlation between Rec114/Mer2 duration and chromosome size and thus also fully explains Rec114/Mer2 overrepresentation on small chromosomes.

However, in an earlier study documenting that Rec114 ChIP-chip signal is higher on the three short chromosomes at 4 h in meiosis, it was stated that the same Rec114 profile was found in a *spo11-Y135F* mutant, which cannot make DSBs (data not shown in ref. [3]; see also **Fig. 1b**). This seems to undermine the homolog engagement hypothesis: there is no homolog engagement without Spo11 activity, so there should be no difference between small and large chromosomes. Furthermore, we found striking DSB protein overrepresentation already at an early time point (2 h) (**Fig. 1c, e and Extended Data Fig. 1d, e**), before synaptonemal complex is likely to have formed[58,59] and before establishment of interhomolog recombination bias[60].

We therefore considered an alternative, namely, that the chromosome size dependence of DSB protein binding is dominated late in prophase by homolog engagement-mediated displacement, but the early pattern is established by a distinct mechanism(s).

2, An artificial short chromosome does not show the boost in Rec114 binding

To carry out the converse of the chromosome-lengthening experiment, we created an artificial short chromosome by engineering a translocation between two medium-size chromosomes (**Extended Data Fig. 6a, b**). The smaller of the derivative chromosomes (der(9), 177 kb) contained the left arm of chr8 (now der(9)L) and the right arm of chr9 (now der(9)R). If our supposition is correct that the shortest chromosomes benefit from an intrinsic boost that does not occur on these segments of chr8 and chr9, then the three-factor regression model should still provide a good fit to the sequences on the artificial short chromosome.

At 2 h, relative Rec114 ChIP density was ~40% higher on der(9)L but slightly lower on der(9)R as compared with the same segments in their normal contexts (**Extended Data Fig. 6c, upper left, and Extended Data Fig. 6d**). The net effect was a modest elevation in chromosome-average Rec114 signal for der(9) relative to the native long chromosomes, but substantially

below the native short trio (**Extended Data Fig. 6c, upper right**). Moreover, a three-factor regression model still predicted Rec114 levels very well on der(9) (note the small residuals for der(9) in **Extended Data Fig. 6e**, right graph). These findings support the conclusion that these segments of chr8 and chr9 do not share the apparent Rec114-binding boost seen on the shortest trio.

Relative Rec114 ChIP density was also elevated on der(9) at 4 h and 6 h, but importantly, the degree of elevation was now closely in line with that on the shortest trio (**Extended Data Fig. 6c, middle and lower panels, and Extended Data Fig. 6f**). Thus, for late Rec114 binding patterns, the artificial short chromosome behaved like a natural short chromosome. This result is readily understood in light of the homolog engagement model, if one assumes that der(9) establishes homolog engagement more slowly and/or less efficiently than either chr8 or chr9, and/or is more strongly affected by a tendency of telomere-adjacent regions to preferentially retain Hop1 in late prophase[33] (discussed below in Section 5).

3, The *hop1 red1* double mutant shows a severe DSB formation defect and drastic change in the distribution of DSB proteins along chromosomes

In the course of these experiments, we found that the strongly diminished Rec114 ChIP signal seen in *hop1* and *red1* single mutants was substantially restored in a *hop1 red1* double mutant. The molecular basis for the restoration is unclear, but it suggests that presence of either Hop1 or Red1 in the absence of the other creates a chromosomal environment that is antagonistic to DSB protein recruitment. Regardless of the mechanism, however, we considered this a useful genetic trick to confirm that the observed loss of Rec114 overrepresentation on short chromosomes in axis mutants was not simply a secondary consequence of crippled Rec114 binding or an artifact of trying to measure extremely weak ChIP signals. Here we provide further characterization of this double mutant.

We measured DSB formation using a Spo11-oligo labeling assay[61] (**Extended Data Fig. 7d**). The double mutant showed timing of labeled Spo11-oligo complexes similar to wild type (maximal signal at 4 h), but at greatly reduced levels (> 20 fold), comparable to reported DSB defects for *hop1* single mutants[62-66]. We infer that Hop1 and Red1 have additional function(s) in DSB formation besides supporting Rec114 binding.

The *hop1* and *red1* single and double mutants showed nuclear division timing similar to or slightly earlier than wild type, while the *rec8* mutant showed a severe defect[62,67-71] that was partially alleviated in the triple mutant (**Extended Data Fig. 7e**). This alleviation may reflect failure to activate Mek1—and failure to inhibit Ndt80 activation—in the absence of Hop1 and Red1[64,72-75]. In addition, the DSB repair defect caused by the *rec8* mutation may have been partially bypassed by the loss of interhomolog bias caused by *hop1* mutation, leading to more rapid repair using the sister chromatid as template, similarly to that seen in *rec8 mek1* and *rec8 red1* mutants[67,71].

To investigate relationships between wild type and axis mutants for Rec114 distributions, we measured correlation coefficients and Euclidean distances between ChIP-seq datasets to generate a correlation matrix and to perform hierarchical clustering (**Extended Data Fig. 7f**). Each dataset was binned in 10-kb windows and standardized prior to analyses. Wild-type Rec114 datasets from 4 and 6 h and Mer2 ChIP from 4 h showed high correlation coefficients ($r > 0.9$),

forming a cluster distinct from other datasets. Rec114 ChIP datasets in wild type at 2 h and all of the 4-h datasets from cells lacking either or both of Red1 and Hop1 also exhibited good correlation ($r > 0.67$; >0.75 without wild type 2 h), forming another cluster.

The separation of these two clusters supports the conclusion that residual Rec114 binding in these axis mutants has a different distribution along and between chromosomes as compared to wild type at similar times, consistent with earlier work[3]. Importantly, this clustering also demonstrates that restoration of Rec114 levels in *red1 hop1* double mutants does not rescue normal spatial distributions, and that the abnormal distribution in single mutants is not a secondary consequence of the greatly diminished chromosomal binding. Moreover, clustering of these axis mutants with the 2-h wild-type time point indicates that the mutants establish a Rec114 distribution that resembles what initially occurs in wild type at or before axis maturation. This is especially interesting for purposes of our study because it highlights the unique behavior of the smallest chromosomes at the earliest time points: the axis mutants resemble the early wild-type sample when considered genome wide, but are very different when focusing on only the small chromosomes.

The *rec8* dataset did not group with either cluster ($r < 0.38$ when compared to all other datasets). This finding further illustrates functional differences between Rec8 and other meiotic axis components[68,71].

To refine this analysis, we further assessed Rec114 distribution relative to transcription units. DSB proteins are enriched at cohesin-favored loci, which are proposed to be determined at least partially by a mechanism where transcription machinery pushes cohesin rings towards transcription termination regions[3,76]. Red1 also shows a similar enrichment at the end of open reading frames (ORFs), dependent on Rec8[17].

ChIP signals were averaged across ORFs (normalized to a length of 1 kb) and the 500 bp up- and downstream, as in a prior analysis[17] (**Extended Data Fig. 7g**). Rec114 and Mer2 ChIP showed the expected enrichment toward the 3′ ends of ORFs at 4 and 6 h (higher than the promoter by 45% and 39%, respectively) but not at 2 h. This enrichment was dependent on Rec8, Hop1 and Red1. The partial restoration of Rec114 ChIP levels in the *hop1 red1* double deletion (with or without *rec8*) did not restore enrichment near ORF ends.

4, Integrating multiple pathways with distinct chromosome size dependencies

To better understand the early pathways, we estimated the absolute contribution of each one to the per-chromosome DSB protein association time (**Fig. 4e**). Because centromere proximity speeds up DSB protein association while telomere proximity delays it, and because these pathways' strengths decay exponentially on different length scales, their chromosome size dependencies differ substantially. The centromere effect is highly non-linear with size, disproportionately influencing the three smallest chromosomes and giving a weaker linear size correlation on the remaining thirteen (**Fig. 4e, panel i**). In contrast, the telomere effect is linearly anticorrelated with size across all chromosomes: the smallest chromosomes are delayed the most but not disproportionately so (**Fig. 4e, panel ii**). Combining these opposing effects leaves the shortest trio with relatively accelerated DSB protein association while the rest of the chromosomes show little difference among themselves (**Fig. 4e, panel iii**). Replication timing correlates very weakly with chromosome size (**Fig. 4e, panel iv**), so adding this effect reinforces

the early advantage of the smallest chromosomes and leaves only a weak size relationship on the larger chromosomes (**Fig. 4e, panel v**).

We initially inferred the existence of a small-chromosome boost because DSB protein association was not fully explained by the combination of replication timing and the centromere and telomere effects (**Fig. 4e, panels v and vi**). Overall, the small-chromosome boost and (to a lesser extent) the centromere effect contribute the most to privileging DSB protein binding on the smallest trio. Replication timing contributes more modestly, while telomeres have a small counter-balancing effect.

It is unclear if the boost is a single mechanism or multiple, or if all three short chromosomes share the same mechanism. If multiple mechanisms are involved, they share a requirement for Hop1 and Red1. We note that the chr1 translocations maintained the boost over one round of meiosis and multiple rounds of mitotic division during strain construction, so we infer that the boost relies on characteristics embedded in the chromosomal DNA sequence, not solely on epigenetic factors.

The homolog engagement pathway defines when pro-DSB factors are removed from chromosomes, and thus dictates the per-chromosome average Rec114 duration. It was previously proposed that the size dependence of homolog engagement is because the speed of homologous pairing and synapsis is governed by the number (not density) of DSBs[2,16,44].

Subramanian, Hochwagen and colleagues suggested a nonexclusive alternative based on their finding that regions near telomeres of most chromosomes (end-adjacent regions, or EARs) are resistant to synapsis-associated downregulation of DSB formation[33]. They proposed that the chromosome size dependence of homolog engagement arises because these telomere-associated regions make up a larger fraction of smaller chromosomes[33] (see also **Supplementary Discussion 5, 6**).

Both models predict an inverse proportional relationship to chromosome size, and indeed a simple inverse proportion model effectively described the chromosome size dependence of DSB protein duration (**Extended Data Fig. 7i**). The net effect of homolog engagement is thus to reinforce the nonlinear relationship between DSB protein binding and chromosome size, such that the smallest trio is highly privileged and the remaining thirteen show a more linear relationship with size (**Extended Data Fig. 7i**).

5, DSB proteins tend to dissociate later near telomeres

EARs experience prolonged DSB formation, apparently because they are relatively resistant to the DSB-suppressive effects of feedback tied to homolog engagement[33]. To test if EARs retain DSB proteins longer (as expected from their tendency to retain axis proteins[33]), we analyzed subchromosomal spatial patterns for Rec114/Mer2 dissociation times and for ChIP densities at a late time point (6 h) (**Extended Data Fig. 8**), similar to our analysis of association times and early ChIP density (**Fig. 2 and Extended Data Fig. 4**). Color-coding dissociation times in 50-kb bins highlighted the late timing of the three shortest chromosomes expected from their whole-chromosome means (e.g., **Fig. 1f**) but also showed that bins near the ends of all chromosomes have late dissociation (**Extended Data Fig. 8a**). Combining the datasets confirmed this conclusion and indicated that the magnitude of delay tends to decay with distance from telomeres (half maximal effect at ~45 kb; **Extended Data Fig. 8b**). By comparison,

pericentromeric regions showed only a modest tendency toward late dissociation that spread much less far (**Extended Data Fig. 8c**).

ChIP densities at 6 h showed related patterns, in that bins with later dissociation tended to show higher ChIP signal late (**Extended Data Fig. 8d**). However, the most telomere-proximal bins tended to have low overall ChIP signal, consistent with the low frequency of DSBs within ~20 kb of telomeres[15,77]. Combined data supported the conclusion that DSB protein abundance in telomere-proximal regions is shaped by overlapping, opposite tendencies: little DSB protein binding within ~20 kb[78] and enrichment up to ~100 kb from chromosome ends (**Extended Data Fig. 8e**). In contrast, centromeres again showed little difference from average (**Extended Data Fig. 8f**). A straightforward interpretation is that the ~20 kb nearest telomeres is intrinsically suppressed for DSB protein accumulation, but the full ~100 kb retains DSB proteins longer than average. A further implication is that the timing of DSB protein dissociation is mechanistically separable from the overall amount of DSB protein binding: even regions that accumulate very little DSB protein binding (and very low DSB numbers) can retain DSB proteins longer than average.

These findings confirm that Rec114 and Mer2 persistence on chromosomes is significantly influenced by the EAR effect. Indeed, dissociation times in the EARs (defined as 20–110 kb from ends[33]) were later on average when compared with interstitial regions (10.1 ± 2.0 min: mean ± SD within three datasets; **Extended Data Fig. 8g**). Consequently, ChIP signals at 6 h tended to be higher in the EARs (fold enrichment relative to interstitial mean was 1.23 ± 0.03 (mean ± SD); **Extended Data Fig. 8h**). Importantly, *zip3* mutation eliminated the late Rec114 overrepresentation in the EARs (**Extended Data Fig. 8h**), supporting the conclusion that the EAR effect is related to ZMM-dependent homolog engagement.

6, DSB protein dissociation is shaped more strongly by chromosome size per se than by telomere proximity

We next used multiple linear regression to systematically investigate the genome-wide patterns of dissociation time for DSB proteins. As explanatory variables, we included proximity to telomeres (which includes the EAR effect as described above), proximity to centromeres (which contributes only weakly (see above)), and association time (which appeared to explain at least some of the variation in dissociation time; **Extended Data Fig. 2a**). Based on the hypothesis that shorter chromosomes require longer to engage with their homologous partners[2,16,44], we also included a separate term to account for this, defined as the reciprocal of chromosome size. The resulting models explained 28% to 53% of the variation in dissociation times (**Extended Data Fig. 9a**) and provided a reasonably good representation of the within-chromosome patterns (**Extended Data Fig. 9b**). Interestingly, data points within ± 100 kb of the rDNA were poorly fit by the model, exhibiting much later dissociation than predicted (**Extended Data Fig. 9c**). These regions thus appear to be under additional layers of regulation[16,79].

We used a similar approach to model ChIP density distributions at 6 h, except that we excluded the association time from the regression analyses because the estimated coefficients were unstable between three datasets. The resulting models explained 41% to 49% of the variation in ChIP density (**Extended Data Fig. 9d**). However, unlike for models of dissociation time, much of the fit relied on data from the shortest chromosomes (R^2 values; compare numbers in parentheses), implying that ChIP density regression models principally describe differences

between long and short chromosomes rather than differences between regions within long chromosomes. Nevertheless, the model did predict overall differences between chromosomes well (**Extended Data Fig. 9e**). Regions near rDNA were not exceptional in this analysis (**Extended Data Fig. 9f**).

In contrast to modeling of DSB protein association (**Extended Data Fig. 5b, d**), these models predicted variation in dissociation time and 6 h ChIP density equally well within short and long chromosomes (**Extended Data Fig. 9g, h**). Thus, no additional feature needs to be invoked to specifically account for behavior of the short trio.

These models allow us to evaluate the relative contribution of each pathway to per-chromosome DSB protein dissociation time and ChIP density at 6 h (**Extended Data Fig. 9i**), similar to our analysis of DSB protein association (**Fig. 4e**). For dissociation time, proximity to centromeres had only a modest impact, as expected. Proximity to telomeres, which includes the EAR effect, had a somewhat greater impact but failed to fully capture chromosome size-related differences. As a result, the modeling term based on chromosome size per se emerged as the largest quantitative contributor even after the telomere effect was accounted for, particularly on the three shortest chromosomes. The tendency toward early association timing counteracted the delays specifically on short chromosomes. Overall, our model predicted chromosomal dissociation time well except for chromosome 12, which exhibited later dissociation than predicted. When considering DSB protein ChIP density, chromosome size emerged as an even more dominant contributor (lower graphs in **Extended Data Fig. 9i**).

Two key conclusions emerge. First, DSB protein dissociation time (and the related aspect of DSB protein density late in prophase) is shaped by the integration of multiple pathways. These pathways are mostly distinct from the ones controlling DSB association time and amount. As a result, the duration of a presumptive DSB-competent state varies in complex and dynamic fashion between chromosomes and between segments within chromosomes. Second, the chromosome size dependency of DSB protein dissociation is only modestly explained by the degree to which EARs make up different fractions of different-sized chromosomes[33]. An additional, more prominent feature(s) related to chromosome size per se is required to fully account for the data. We previously proposed that the kinetics of chromosome pairing is such a feature[2,16], supported by estimates of lifespans of resected DSBs[44]. However, we do not exclude the possibility that as-yet unknown processes also contribute.

7, Establishing and realizing DSB potential

Cells establish “DSB potential” through control of the timing of DSB-promoting factors on chromosomes, but the amount of DSB proteins is probably also important. It is also likely that control of amount and timing are related but separable. For example, we envision that higher affinity binding sites outcompete weaker ones at early times when DSB proteins are first induced and at limiting concentrations, so high affinity sites will also tend to be earlier ones. Conversely, segments that are early for other reasons (e.g., proximity to early-firing replication origins) may not necessarily accumulate the highest levels of Rec114 etc., but would have a head start over other regions.

Once established, DSB potential must be realized in the form of DSBs and, eventually, recombination. Just as DSB potential is the net result of multiple integrated pathways, so too are

DSB and recombination frequencies the net result of many influences. A good example of this complexity is provided by pericentromeric regions, where multiple, often mutually antagonistic, pathways work on different size scales to control DSB formation and recombination. Crossovers near centromeres can provoke missegregation[80], so local DSB protein enrichment could be deleterious. However, centromere-bound kinetochore components suppress DSB formation at short range (~6-kb scale) and Rec8 inhibits interhomolog recombination for DSBs within ~20 to 50 kb of centromeres[81]. Interestingly, suppression of interhomolog recombination and centromeric enrichment of Rec114 work on similar size scales and both require Rec8, suggesting they may be mechanistically related.

8, Perturbing the DSB assurance network leads to chromosome size dependent missegregation

A motivation for this study was the supposition that the DSB allocation systems we are examining work combinatorially to ensure enough DSBs and thus crossovers. If so, then disrupting these pathways should result in missegregation, with short chromosomes being the most sensitive. One critical module making the system robust is a reactive pathway where activation of Mec1/Tel1 kinases by DSB formation results in activation of Mek1 kinase, which channels DSBs predominantly into interhomolog recombination and inhibits Ndt80 activity[82]. Ndt80 is a transcription factor controlling pachytene exit, which is thought to include termination of a DSB-permissive state through disassembly of meiotic chromosome structures including the DSB formation machinery[2,7,16,34-37,72,73]. Until Ndt80 is expressed, chromosomes are able to continue to make DSBs and carry out pairing and recombination, until or unless inhibited by negative feedback tied to homolog engagement[2,16]. Thus, timely expression of Ndt80 is key. Moreover, these reactive pathways act homeostatically, which means that they allow cells to tolerate changes in DSB number resulting from perturbation in the proactive pathways, minimizing detectable crossover defects and missegregation.

Therefore, to test the importance of DSB control for ensuring chromosome segregation, we wished to set up a system to attenuate multiple layers of the control. We did this by comparing segregation of a mid-sized chromosome (chr5) with that of a natural small chromosome (chr6) and the artificial small chromosome that lacks the small-chromosome boost (der(9)), and by placing Ndt80 under the control of the Gal4-ER system[52]. This strain expresses Ndt80 upon addition of β-estradiol irrespective of homolog engagement state, and thus can be used to prematurely terminate DSB potential. To monitor both crossovers and chromosome segregation, we integrated spore-autonomous fluorescent markers[39] on der(9) (**Extended Data Fig. 10a–c**). Then, to compare sensitivities of different chromosomes to premature Ndt80 expression, we integrated the fluorescent markers on chr5, chr6, and der(9) (**Fig. 4f and Extended Data Fig. 10d, e**).

9, Karyotype constrains the DSB landscape in yeast and beyond

Our findings demonstrate how complex mechanisms collaborate to mitigate the missegregation risk of the smallest chromosomes. An alternative could be to avoid having short chromosomes altogether, but the apparently risky karyotype of *S. cerevisiae* is an ancient and evolutionarily successful one. This stability may imply that having these short chromosomes carries a fitness benefit that remains to be elucidated.

Chr3 has additional characteristics that shape its DSB landscape. Recombination is lower than genome average in the 86 kb from the centromere (*CEN3*) to the mating type locus (*MAT*), mostly because this is a cold zone for DSB formation[83]. It has been argued that linkage of *MAT* to *CEN3* favors maintenance of heterozygosity for centromere-linked genes after mating of spores from the same tetrad (automixis), and/or promotes formation of spores of the opposite mating type when sporulation produces a dyad instead of a tetrad under nutrient limitation[84-86]. *CEN3–MAT* linkage may also be important to reduce likelihood of loss of heterozygosity at *MAT* in diploids that return to vegetative growth after transiently entering meiosis (M. Lichten, personal communication). Thus, it appears that pressure to maintain *CEN3–MAT* linkage has selected for suppression of DSB formation across this region throughout the *Saccharomyces* clade[26]. As a consequence, DSB frequencies must be elevated even more in the flanking regions to compensate for low DSB frequency between *CEN3* and *MAT*. This compensation involves high-level recruitment of axis and DSB proteins[3,32] (this study). Indeed, the three-factor regression model underperformed to an even greater extent on the parts of chr3 excluding *CEN3–MAT* than it did for chr1 and chr6 (**Extended Data Fig. 10f**), indicative of an even stronger boost of Rec114 binding.

Boosting DSB protein binding is not unique to yeast. This strategy is also used in mammals to accomplish a similar end, i.e., ensuring high-level DSB formation in small chromosome segments that would otherwise risk missegregation. In most eutherian mammals, accurate segregation of the sex chromosomes in male meiosis requires that X and Y recombine, but they share only a short region(s) of homology called the pseudoautosomal region (PAR)[87]. In mice, the <1 Mb-long PAR is too small to acquire a DSB in every meiosis if it behaved like a typical genomic segment (genome average is only 1 DSB per ~10 Mb), so the PAR is exceptionally hot for DSB formation[29,88-90]. Similar to the small chromosomes in yeast, preferential DSB formation in the PAR relies on recruitment of high levels of REC114, MEI4, and IHO1 (the mouse Mer2 ortholog) dependent on DNA elements within the PAR[28].

It is thus a general principle that the recombination landscape can be shaped profoundly by the intersection between karyotype and the demands of meiotic chromosome segregation, particularly the requirement for at least one DSB per chromosome pair.

Supplementary Table 1. Oligonucleotides

TL#1AF GTTCGGTTACTTTATTCTGCTTTAACGCCATTATGATTATACACATTGTACTTGACGTTCGTTCGACTGAT GAGC
TL#1AR TAATGTGAAATAAAATAAAGGTTTTAATATACAGGTTAAAAAATAAGTAAAATTCGGTCGAAAAAAGAAAA GGAGAGG
TL#1BF ATCATTATATATTATCTACTTGCATGAACACTTTAATCACGCTTATTTAACGTTTTAAGAGCTTGGTGAGC GC
TL#1BR TCCACTATATAAAACAAAGCACAATTGCACCTCTGATCTTTTAATCTTAAGAGCAATGAACCCAATAACG AAATC
gRNA (YHL012w) CATGATTCCTCTTACATAGTggg
gRNA (URM1) AATCACAAGTTAGATAACGTagg
Donor DNA (YHL012w_NAS2_temp) GAGAAACTTTTGGGTAAAATGCATGAATAAAGTTTTCTTCTATTCCCACTCGTAGGTAATATGCAGATAG TATAAAAAGTAATAGTAATAACTGGATTGG
Donor DNA (URM1_PRS3_temp) TATATATATATAAAGTGCTGTACAGCTTGAATGAATCACAAGTTAGATAAATGTAAGAGGAATCATGTATC CTCACAGAAAAAAAAAACTGGAGCACATT
chr1LF(BDH1) ATGAGAGCCTTAGCGTATTTCG
chr1LR(BDH1) CATGTGTGACGCAGTTTAGCCTC
chr1RF(SWH1) ACCGTTGATTTCATCCAGAAGC
chr1RR(SWH1) TTCGTCGGCGTCAGAATCCTC
chr4LF(LRG1) GATCGCTGAACACTGCATCTCC
chr4LR(LRG1) ATCAGAAATGCAAGAAGCTGCCT
chr4RF(FDC1) TCCAAATCTCGAAGTAGGTG
chr4RR(FDC1) AAGATAAGCCAAAGAGCCTGAG
chr8LF(EFM1) GATAACTGCTTACAATGGGCTC
chr8LR(EFM1) CTTCGTTCAGATTGGTGCTGTC
chr8RF(SET5) GCAAAGCTATTTGGTGCAGTG
chr8RR(SET5) TTATCTTTCATCCACTGCGACC
chr9LF(YIL166c) TTCATAAAGCAGAGCGTTGGAG
chr9LR(YIL166c) ATTTATTAGCAGCAGGGCTTGACC
chr9RF(GTT1) TGGTTGGACCATTCCAGAGC
chr9RR(GTT1) CCTTAGAAGCAGCATACGACTC

inf9RightRFPF GCACCATATCGACTAGCACTGTGTTATTCTTCTTGTTACCU
inf9RightRFPR ACGGCCTTACGACGTTGTGTTACTGTGTGGGACTG
TF_RFP_cen6F CTTTTAGAAATCACATTTAAGGGGAAGTTTTAAATCATTCATAAATATCAgcaactagcaaggagaattagaggac
TF_RFP_cen6R CTGTACAGAGTTATCAAAAACCGGAGAAAATGATGTTTATGTAAATGCATctaccctatgaacatattccattttgtaatttcg
cen6_RFP_check1F TGGCTAACTACATGGCATACG
cen1_RFP_check1R GAACTGTCCTCTAATTCTCCTTGC
cen1_RFP_check2F ATGCTGTCGCCGAAGAAGTTAAG
cen6_RFP_check2R TGGATGCAGTCCTTCTCAATG
TF_GFP_cen9v3F GAGAAACTTTTGGGTAAAATGCATGAATAAAGTTTTCTTCTATTCCCACTAGCTTGCCTCGTCCCC
TF_GFP_cen9v3R CCAATCCAGTTATTACTATTACTTTTTATACTATCTGCATATTACCTACGgtgggatgagcttggagcag
cen9_GFP_check3F GGATTATTACCTTCAATCGACTTGG
cen9_GFP_check1v2R CGCACGTCAAGACTGTCAAGG
cen9_GFP_check2F TCTTCCTGCTCCAAGCTCATC
cen9_GFP_check3R AAGACATCGCTAACACCTTCGAG
TF_CFP_cen5F AAAAAAGACAATAAGATTCAAGTCGTTAAAAACTAAACCATATATAAAATgaggatacactatacaggatccaaagaat
TF_CFP_cen5R TACCTGATTGTGTTTATTTATATTTTTTGCCAAACTAAGTACTGCAATAGAGATCTGTTTAGCTTGCCTCGTC
cen5_CFP_check1F 5197 GGATGATAGGTGGCGCACTTG 5217
cen5_CFP_check1R TTGTGCTGCCAGTATCCTTATCC
cen5_CFP_check2F CGCACGTCAAGACTGTCAAGG
cen5_CFP_check2R CGTCACGACTTCCTCTGTTGG
TF_CFP_chr8LF TTCATACTAATCAATATGTACACAGGCTTCACATTAGAACATCATATATTAGATCTGTTTAGCTTGCCTCGTC
TF_CFP_chr8LR AGCATGTATATGAACAAAAATGTATTATCTGGATTTTAAGTTATCGCTTTgaggatacactatacaggatccaaagaat
chr8L_CFP_check1F CATGGTGTCATTAGCGTGAAAG
chr8L_CFP_check1R GACTGTCAAGGAGGGTATTCTGG
chr8L_CFP_check2F TGTGCTGCCAGTATCCTTATCC

chr8L_CFP_check2R GAACAAAAATGTATTATCTGGATTTTAAGTTATCGC
chr9R_RFP_check1F AGATAAGGAAGCCGCGATGG
chr9R_RFP_check1R TGCTGTCGCCGAAGAAGTTAAG
chr9R_RFP_check2F GAACTGTCCTCTAATTCTCCTTGC
chr9R_RFP_check2R TTCTCAAGTAGTGGCGGCTC

Supplementary Table 2. Yeast strains

Strain number: genotype	Source
SKY2897: *MATa/alpha, ho::LYS2/", lys2/", ura3::pRS306/", leu2::hisG/", arg4/", REC114-myc8::ura3::HphMX6/"*	[18]
SKY3371: *MATa/alpha, ho::LYS2/", lys2/", ura3::pRS306/", leu2/", arg4-nsp,bgl/", ars305Δ/", ars306Δ/", ars307-T108569G/", REC114-myc8::ura3::HphMX6/"*	[18]
SKY3729: *MATa/alpha, ho::LYS2/", lys2/", ura3::pRS306/", leu2::hisG/", arg4-Nsp/", REC114-myc8::ura3::HphMX6/", tof1Δ::KanMX/"*	[18]
SKY3734: *MATa/alpha, ho::LYS2/", lys2/", ura3::pRS306/", leu2/", arg4-nsp,bgl/", ars305Δ/", ars306Δ/", ars307-T108569G/", tof1Δ::KanMX/", REC114-myc8::ura3::HphMX6/"*	[18]
SKY2863: *MATa/alpha, ho::LYS2/", lys2/", ura3/", leu2/", arg4-nsp,bgl/", ars305Δ/", ars306Δ/", ars307-T108569G/", mer2::pKH35(MER2-myc5,URA3)::HphMX/"*	This study
SKY5660: *MATa/alpha, ho::LYS2/", lys2/", ura3/", leu2::hisG/", arg4/ARG4, REC114-myc8::ura3::HphMX6/", zip3Δ::hphMX4/"*	This study
SKY5689: *MATa/alpha, ho::LYS2/", lys2/", ura3/", leu2::hisG/", his3::hisG/", trp1::hisG/", REC114-myc8::ura3::HphMX6/", translocation: chr4-SLX5:HIS3:KlURA3:TRP1:MDM10-chr1/"; chr1-SWC3:Klura3(part):YDL012c-chr4/"*	This study
SKY5683: *MATa/alpha, ho::LYS2/", lys2/", ura3/", leu2::hisG/", REC114-myc8::ura3::HphMX6/", translocation: chr8-(80472)-chr9/"; chr9-(342921)-chr8/"*	This study
SKY 5998: *MATa/alpha, ho::LYS2/", lys2/", ura3/", leu2::hisG/", hop1D::LEU2/", Rec114-myc8::URA/"*	This study
SKY5999: *MATa/alpha, ho::LYS2/", lys2/", ura3/", leu2::hisG/", red1Δ::HphMX/", Rec114-myc8::URA/"*	This study
SKY6027: *MATa/alpha, ho::LYS2/", lys2/", ura3/", leu2::hisG/", arg4-Nsp/ARG4, rec8Δ::KanMX6/", Rec114-myc8::URA/"*	This study
SKY6030: *MATa/alpha, ho::LYS2/", lys2/", ura3/", leu2::hisG/", arg4-Nsp/ARG4, hop1D::LEU2/", red1Δ::HphMX/", Rec114-myc8::URA/"*	This study
SKY6031: *MATa/alpha, ho::LYS2/", lys2/", ura3/", leu2::hisG/", arg4-Nsp/ARG4, hop1D::LEU2/", red1Δ::HphMX/", rec8Δ::KanMX6/", Rec114-myc8::URA/"*	This study
SKY7023: *MATa/alpha, ho::LYS2/", lys2/", ura3::P_{GPD1}-GAL4(848)-ER::URA3/", leu2::hisG/",his3::hisG/", trp1::hisG/", translocation: chr8-(80472)-chr9(YHL048w-$P_{YKL050c}$-CFP-NatMX: NAS2: YPS6-$P_{YKL050c}$-RFP-LEU2)/chr8-(80472)-chr9(YHL048w: NAS2-$P_{YKL050c}$-GFP*-KanMX: YPS6); chr9-(342921)-chr8(P_{GAL}-NDT80::TRP1)/"*	This study
SKY7034: *MATa/alpha, ho::LYS2/", lys2/", ura3::P_{GPD1}-GAL4(848)-ER::URA3/", leu2::hisG/",his3::hisG/", trp1::hisG/", translocation: chr8-(80472)-chr9(NAS2)/chr8-(80472)-chr9(NAS2-$P_{YKL050c}$-GFP*-KanMX); chr9-(342921)-chr8(P_{GAL}-NDT80::TRP1)/", MSH4-$P_{YKL050c}$-RFP-LEU2/MSH4, GIM4-$P_{YKL050c}$-CFP-NatMX/GIM4*	This study

Supplementary Table 3. Multiple regression results for dissociation time

Dataset	Variable	Coefficient	Std.error (coef)	Beta	Std.error (beta)	*t* statistic	*P* value
Rec114 ChIP *ARS*+	Association	0.062	0.045	0.06	0.042	1.39	1.64E-01
	Chr size	1.70E+04	9.36E+03	0.08	0.045	1.82	7.01E-02
	Cen effect	0.204	0.046	0.17	0.039	4.44	1.13E-05
	Tel effect	0.162	0.016	0.45	0.045	10.16	3.72E-22
	Intercept	4.790	0.120	0	0.038	0	1
Rec114 ChIP *ARS*+	Association	0.092	0.054	0.09	0.050	1.70	8.93E-02
w/o short chr	Chr size	4.71E+04	1.84E+04	0.12	0.045	2.56	1.08E-02
	Cen effect	-0.289	0.083	-0.16	0.046	-3.47	5.72E-04
	Tel effect	0.166	0.027	0.31	0.050	6.09	2.36E-09
	Intercept	4.663	0.142	0	0.042	0	1
Rec114 ChIP *ars*Δ	Association	0.513	0.054	0.34	0.036	9.45	1.07E-19
	Chr size	8.86E+04	1.08E+04	0.30	0.036	8.22	1.55E-15
	Cen effect	0.469	0.058	0.27	0.033	8.04	5.72E-15
	Tel effect	0.171	0.015	0.41	0.035	11.50	1.68E-27
	Intercept	3.205	0.137	0	0.031	0	1
Rec114 ChIP *ars*Δ	Association	0.891	0.066	0.59	0.043	13.58	5.34E-36
w/o short chr	Chr size	1.19E+05	1.99E+04	0.22	0.037	5.97	4.43E-09
	Cen effect	-1.264	0.113	-0.47	0.042	-11.16	5.47E-26
	Tel effect	0.041	0.026	0.06	0.039	1.59	1.12E-01
	Intercept	2.257	0.161	0	0.035	0	1
Mer2 ChIP *ars*Δ	Association	0.399	0.037	0.35	0.032	10.90	2.83E-25
	Chr size	6.60E+04	6.04E+03	0.35	0.032	10.94	1.97E-25
	Cen effect	0.191	0.031	0.18	0.030	6.11	1.87E-09
	Tel effect	0.096	0.008	0.39	0.033	11.90	2.30E-29
	Intercept	3.653	0.092	0	0.028	0	1
Mer2 ChIP *ars*Δ	Association	0.671	0.045	0.58	0.039	14.80	7.63E-42
w/o short chr	Chr size	1.09E+05	1.20E+04	0.31	0.034	9.06	2.33E-18
	Cen effect	-0.562	0.059	-0.36	0.037	-9.61	2.66E-20
	Tel effect	0.006	0.015	0.01	0.036	0.41	6.84E-01
	Intercept	2.943	0.111	0	0.032	0	1

Supplementary Table 4. Multiple regression results for ChIP density at 6 h

Dataset	Variable	Coefficient	Std.error (coef)	Beta	Std.error (beta)	*t* statistic	*P* value
Rec114 ChIP *ARS*+	Chr size	5.12E+03	3.23E+02	0.56	0.035	15.87	3.04E-46
	Cen effect	0.002	0.002	0.03	0.032	0.89	3.75E-01
	Tel effect	0.006	0.001	0.26	0.035	7.60	1.47E-13
	Intercept	0.024	0.000	0	0.032	0	1
Rec114 ChIP *ARS*+	Chr size	3.30E+03	5.73E+02	0.25	0.044	5.75	1.57E-08
w/o short chr	Cen effect	0.002	0.002	0.03	0.041	0.77	4.44E-01
	Tel effect	0.006	0.001	0.33	0.044	7.68	9.38E-14
	Intercept	0.026	0.001	0	0.040	0	1
Rec114 ChIP *ars*Δ	Chr size	3.72E+03	2.39E+02	0.55	0.035	15.58	2.22E-45
	Cen effect	0.001	0.002	0.02	0.033	0.68	4.99E-01
	Tel effect	0.003	0.001	0.23	0.035	6.49	2.01E-10
	Intercept	0.017	0.000	0	0.032	0	1
Rec114 ChIP *ars*Δ	Chr size	2.09E+03	3.95E+02	0.23	0.043	5.28	1.89E-07
w/o short chr	Cen effect	0.001	0.002	0.01	0.041	0.30	7.64E-01
	Tel effect	0.003	0.000	0.28	0.043	6.60	1.02E-10
	Intercept	0.019	0.000	0	0.040	0	1
Mer2 ChIP *ars*Δ	Chr size	3.76E+03	2.53E+02	0.51	0.034	14.88	1.24E-42
	Cen effect	0.006	0.002	0.11	0.032	3.39	7.35E-04
	Tel effect	0.005	0.001	0.28	0.034	8.22	1.37E-15
	Intercept	0.013	0.000	0	0.032	0	1
Mer2 ChIP *ars*Δ	Chr size	2.15E+03	4.29E+02	0.20	0.041	5.01	7.52E-07
w/o short chr	Cen effect	0.006	0.002	0.12	0.039	3.17	1.63E-03
	Tel effect	0.004	0.001	0.32	0.040	7.97	9.48E-15
	Intercept	0.015	0.001	0	0.039	0	1

Supplementary Table 5. Multiple regression results for association and ChIP density at 2h

Dataset	Variable	Coefficient	Std.error (coef)	Beta	Std.error (beta)	*t* statistic	*P* value
Rec114 ChIP *ARS*+	Rep index	0.521	0.0723	0.32	0.044	7.21	2.1E-12
Association time	Cen effect	0.075	0.0116	0.29	0.044	6.48	2.2E-10
	Tel effect	0.104	0.0133	0.28	0.035	7.83	3.0E-14
	Intercept	2.562	0.0051	0	0.035	0	1
Rec114 ChIP *ars*Δ	Rep index	0.333	0.0535	0.21	0.034	6.23	9.7E-10
Association time	Cen effect	0.146	0.0091	0.55	0.034	16.08	9.0E-48
	Tel effect	0.070	0.0106	0.20	0.030	6.56	1.3E-10
	Intercept	2.402	0.0043	0	0.030	0	1
Mer2 ChIP *ars*Δ	Rep index	0.265	0.0728	0.13	0.035	3.65	0.0003
Association time	Cen effect	0.100	0.0075	0.46	0.035	13.32	1.8E-35
	Tel effect	0.091	0.0095	0.31	0.033	9.63	1.8E-20
	Intercept	2.432	0.0039	0	0.032	0	1
Rec114 ChIP *ARS*+	Rep index	-0.005	0.0010	-0.19	0.039	-4.97	8.9E-07
ChIP density at 2 h	Cen effect	0.002	0.0002	0.52	0.038	13.41	5.3E-36
	Tel effect	-0.001	0.0004	-0.09	0.032	-2.73	0.0065
	Intercept	0.008	0.0001	0	0.032	0	1
Rec114 ChIP *ars*Δ	Rep index	-0.020	0.0050	-0.16	0.038	-4.08	5.2E-05
ChIP density at 2 h	Cen effect	0.011	0.0009	0.49	0.038	13.05	2.2E-34
	Tel effect	0.001	0.0019	0.01	0.034	0.40	0.69
	Intercept	0.016	0.0004	0	0.033	0	1
Mer2 ChIP *ars*Δ	Rep index	-0.018	0.0091	-0.07	0.038	-1.95	0.051
ChIP density at 2 h	Cen effect	0.014	0.0010	0.51	0.037	13.65	4.5E-37
	Tel effect	0.002	0.0023	0.03	0.035	0.90	0.37
	Intercept	0.025	0.0005	0	0.034	0	1
Rec114 ChIP	Rep index	-0.012	0.0041	-0.11	0.040	-2.88	0.0041
Translocation	Cen effect	0.006	0.0005	0.46	0.040	11.52	7.3E-28
btw chr1-chr4	Tel effect	0.000	0.0012	0.01	0.035	0.16	0.87
ChIP density at 2 h	Intercept	0.012	0.0002	0	0.035	0	1
Rec114 ChIP	Rep index	-0.033	0.0165	-0.08	0.041	-1.99	0.047
Translocation	Cen effect	0.021	0.0021	0.40	0.041	9.70	9.9E-21
btw chr8-chr9	Tel effect	0.004	0.0046	0.03	0.037	0.82	0.41
ChIP density at 2 h	Intercept	0.052	0.0010	0	0.037	0	1
Rec114 ChIP	Rep index	-0.037	0.0183	-0.09	0.045	-2.04	0.042
S. mikatae	Cen effect	0.009	0.0018	0.23	0.045	5.01	7.3E-07
ChIP density at 2 h	Tel effect	0.016	0.0039	0.16	0.040	4.08	5.1E-05
	Intercept	0.044	0.0009	0	0.039	0	1

Supplementary Table 6. Fluorescent spore assay (SKY7023)

	Time of *NDT80* induction							
	3 h	**3.5 h**	**4 h**	**4.5 h**	**5 h**	**5.5 h**	**6 h**	**7 h**
TT (CFP-GFP)	60	58	73	90	107	103	110	129
TT (GFP-RFP)	49	63	53	68	97	102	88	110
PD (CFP-GFP)	103	116	95	84	72	75	61	48
PD (GFP-RFP)	114	113	117	110	81	77	85	59
NPD (CFP-GFP)	3	5	5	8	6	10	11	11
NPD (GFP-RFP)	3	3	3	3	7	9	10	19
CO# in the CFP-GFP interval	78	88	103	138	143	163	176	195
CO# in the GFP-RFP interval	67	81	71	86	139	156	148	224
Total # of COs	145	169	174	224	282	319	324	419
Marker loss or gain	3	0	2	2	13	7	14	10
Total number of tetrad analyzed	197	200	198	198	187	193	186	190
Observed MINDJ	31	21	25	16	2	5	3	2
Corrected MINDJ	30.955	20.925	24.925	15.88	1.79	4.55	2.45	0.955
Observed E0	78	76	63	49	37	38	26	12
Corrected E0	77.955	75.925	62.925	48.88	36.79	37.55	25.45	10.955

A total 200 tetrads were scored per time point. MINDJ: MI nondisjunction, E0: nonexchange, TT: tetratype, PD: parental ditype, NPD: nonparental ditype.

Supplementary Table 7. Fluorescent spore assay (SKY7034)

		Time of *NDT80* induction	
		4 h	**5 h**
Total number of tetrad analyzed		563	516
Number of tetrad with MI nondisjunction	None	495	501
	GFP	31	7
	RFP	13	5
	CFP	11	0
	GFP and RFP	12	3
	RFP and CFP	1	0
	GFP and CFP	0	0
	RFP, GFP and CFP	0	0
MI nondisjunction rate	GFP	7.6% (43/563)	1.9% (10/516)
	RFP	4.6% (26/563)	1.6% (8/516)
	CFP	2.1% (12/563)	0% (0/516)

Extended Figure 5f and Extended Figure 6b

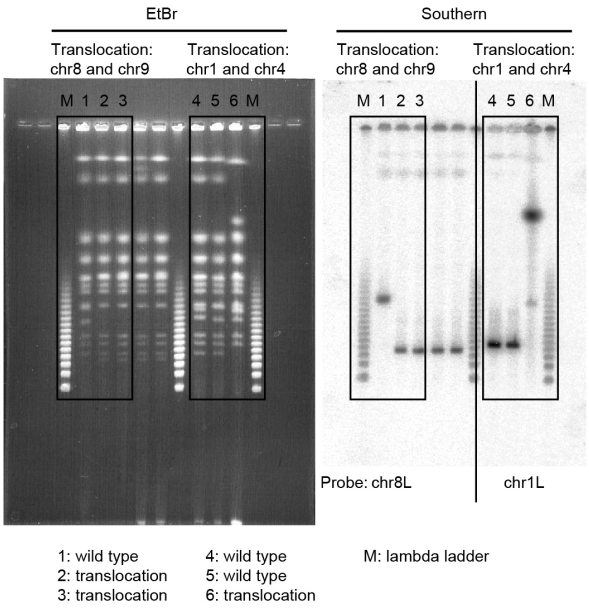

Extended Figure 7d

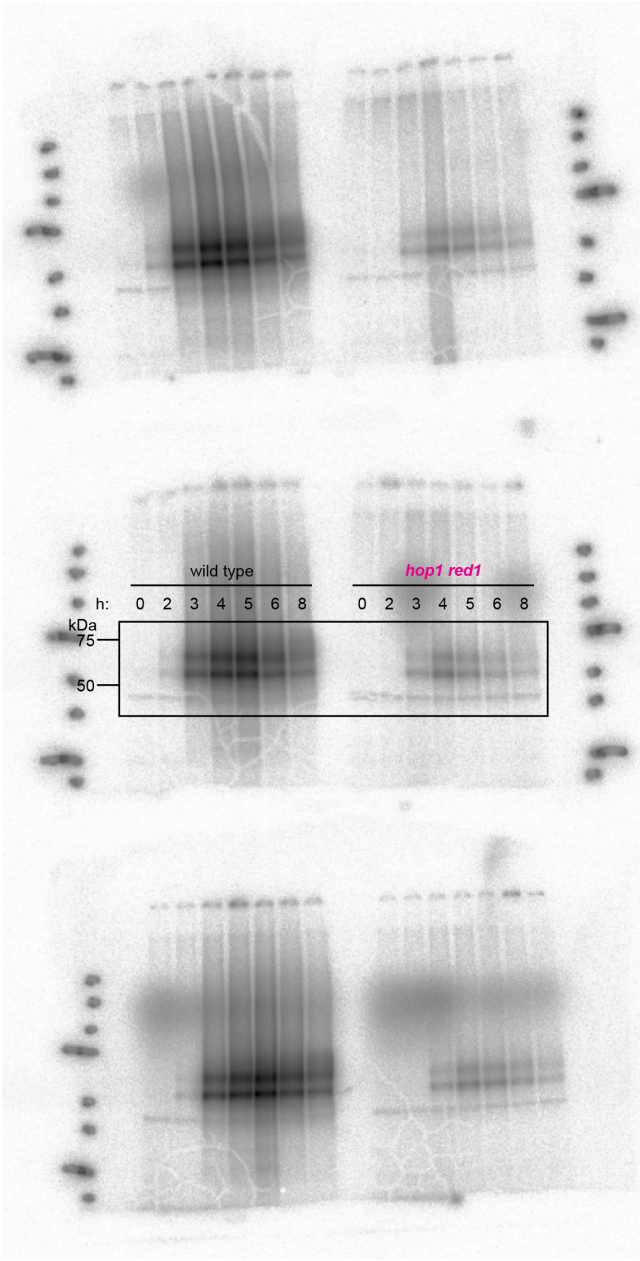

Supplementary Figure 1. Original source images.

Supplementary References:

57 Kumar, R. *et al.* MEI4 - a central player in the regulation of meiotic DNA double-strand break formation in the mouse. *J Cell Sci* **128**, 1800-1811, doi:10.1242/jcs.165464 (2015).

58 Padmore, R., Cao, L. & Kleckner, N. Temporal comparison of recombination and synaptonemal complex formation during meiosis in S. cerevisiae. *Cell* **66**, 1239-1256 (1991).

59 Henderson, K. A. & Keeney, S. Tying synaptonemal complex initiation to the formation and programmed repair of DNA double-strand breaks. *Proc Natl Acad Sci U S A* **101**, 4519-4524, doi:10.1073/pnas.0400843101 0400843101 [pii] (2004).

60 Joshi, N., Brown, M. S., Bishop, D. K. & Borner, G. V. Gradual implementation of the meiotic recombination program via checkpoint pathways controlled by global DSB levels. *Mol Cell* **57**, 797-811, doi:10.1016/j.molcel.2014.12.027 (2015).

61 Neale, M. J. & Keeney, S. Clarifying the mechanics of DNA strand exchange in meiotic recombination. *Nature* **442**, 153-158, doi:nature04885 [pii] 10.1038/nature04885 (2006).

62 Carballo, J. A., Johnson, A. L., Sedgwick, S. G. & Cha, R. S. Phosphorylation of the axial element protein Hop1 by Mec1/Tel1 ensures meiotic interhomolog recombination. *Cell* **132**, 758-770, doi:S0092-8674(08)00135-9 [pii] 10.1016/j.cell.2008.01.035 (2008).

63 Mao-Draayer, Y., Galbraith, A. M., Pittman, D. L., Cool, M. & Malone, R. E. Analysis of meiotic recombination pathways in the yeast Saccharomyces cerevisiae. *Genetics* **144**, 71-86 (1996).

64 Niu, H. *et al.* Partner choice during meiosis is regulated by Hop1-promoted dimerization of Mek1. *Mol Biol Cell* **16**, 5804-5818, doi:10.1091/mbc.e05-05-0465 (2005).

65 Pecina, A. *et al.* Targeted stimulation of meiotic recombination. *Cell* **111**, 173-184, doi:10.1016/s0092-8674(02)01002-4 (2002).

66 Woltering, D. *et al.* Meiotic segregation, synapsis, and recombination checkpoint functions require physical interaction between the chromosomal proteins Red1p and Hop1p. *Mol Cell Biol* **20**, 6646-6658 (2000).

67 Callender, T. L. & Hollingsworth, N. M. Mek1 suppression of meiotic double-strand break repair is specific to sister chromatids, chromosome autonomous and independent of Rec8 cohesin complexes. *Genetics* **185**, 771-782, doi:10.1534/genetics.110.117523 (2010).

68 Klein, F. *et al.* A central role for cohesins in sister chromatid cohesion, formation of axial elements, and recombination during yeast meiosis. *Cell* **98**, 91-103, doi:10.1016/S0092-8674(00)80609-1 (1999).

69 Markowitz, T. E. *et al.* Reduced dosage of the chromosome axis factor Red1 selectively disrupts the meiotic recombination checkpoint in Saccharomyces cerevisiae. *PLoS Genet* **13**, e1006928, doi:10.1371/journal.pgen.1006928 (2017).

70 Schwacha, A. & Kleckner, N. Interhomolog bias during meiotic recombination: meiotic functions promote a highly differentiated interhomolog-only pathway. *Cell* **90**, 1123-1135, doi:10.1016/s0092-8674(00)80378-5 (1997).

71 Kim, K. P. *et al.* Sister cohesion and structural axis components mediate homolog bias of meiotic recombination. *Cell* **143**, 924-937, doi:10.1016/j.cell.2010.11.015 (2010).

72 Okaz, E. *et al.* Meiotic prophase requires proteolysis of M phase regulators mediated by the meiosis-specific APC/CAma1. *Cell* **151**, 603-618, doi:10.1016/j.cell.2012.08.044 (2012).

73 Prugar, E., Burnett, C., Chen, X. & Hollingsworth, N. M. Coordination of Double Strand Break Repair and Meiotic Progression in Yeast by a Mek1-Ndt80 Negative Feedback Loop. *Genetics* **206**, 497-512, doi:10.1534/genetics.117.199703 (2017).

74 Wan, L., de los Santos, T., Zhang, C., Shokat, K. & Hollingsworth, N. M. Mek1 kinase activity functions downstream of RED1 in the regulation of meiotic double strand break repair in budding yeast. *Mol Biol Cell* **15**, 11-23, doi:10.1091/mbc.e03-07-0499 (2004).

75 Xu, L., Ajimura, M., Padmore, R., Klein, C. & Kleckner, N. NDT80, a meiosis-specific gene required for exit from pachytene in Saccharomyces cerevisiae. *Mol Cell Biol* **15**, 6572-6581, doi:10.1128/mcb.15.12.6572 (1995).

76 Lengronne, A. *et al.* Cohesin relocation from sites of chromosomal loading to places of convergent transcription. *Nature* **430**, 573-578, doi:10.1038/nature02742 (2004).

77 Blitzblau, H. G. & Hochwagen, A. Genome-wide detection of meiotic DNA double-strand break hotspots using single-stranded DNA. *Methods Mol Biol* **745**, 47-63, doi:10.1007/978-1-61779-129-1_4 (2011).

78 Mieczkowski, P. A., Dominska, M., Buck, M. J., Lieb, J. D. & Petes, T. D. Loss of a histone deacetylase dramatically alters the genomic distribution of Spo11p-catalyzed DNA breaks in Saccharomyces cerevisiae. *Proc Natl Acad Sci U S A* **104**, 3955-3960, doi:10.1073/pnas.0700412104 (2007).

79 Vader, G. *et al.* Protection of repetitive DNA borders from self-induced meiotic instability. *Nature* **477**, 115-119, doi:10.1038/nature10331 (2011).
80 Rockmill, B., Voelkel-Meiman, K. & Roeder, G. S. Centromere-proximal crossovers are associated with precocious separation of sister chromatids during meiosis in Saccharomyces cerevisiae. *Genetics* **174**, 1745-1754, doi:10.1534/genetics.106.058933 (2006).
81 Vincenten, N. *et al.* The kinetochore prevents centromere-proximal crossover recombination during meiosis. *Elife* **4**, doi:10.7554/eLife.10850 (2015).
82 Hollingsworth, N. M. & Gaglione, R. The meiotic-specific Mek1 kinase in budding yeast regulates interhomolog recombination and coordinates meiotic progression with double-strand break repair. *Curr Genet* **65**, 631-641, doi:10.1007/s00294-019-00937-3 (2019).
83 Baudat, F. & Nicolas, A. Clustering of meiotic double-strand breaks on yeast chromosome III. *Proc Natl Acad Sci U S A* **94**, 5213-5218, doi:10.1073/pnas.94.10.5213 (1997).
84 Knop, M. Evolution of the hemiascomycete yeasts: on life styles and the importance of inbreeding. *Bioessays* **28**, 696-708, doi:10.1002/bies.20435 (2006).
85 Lacefield, S., Magendantz, M. & Solomon, F. Consequences of defective tubulin folding on heterodimer levels, mitosis and spindle morphology in Saccharomyces cerevisiae. *Genetics* **173**, 635-646, doi:10.1534/genetics.105.055160 (2006).
86 Taxis, C. *et al.* Spore number control and breeding in Saccharomyces cerevisiae: a key role for a self-organizing system. *J Cell Biol* **171**, 627-640, doi:10.1083/jcb.200507168 (2005).
87 Raudsepp, T., Das, P. J., Avila, F. & Chowdhary, B. P. The pseudoautosomal region and sex chromosome aneuploidies in domestic species. *Sex Dev* **6**, 72-83, doi:10.1159/000330627 (2012).
88 Lange, J. *et al.* The Landscape of Mouse Meiotic Double-Strand Break Formation, Processing, and Repair. *Cell* **167**, 695-708 e616, doi:10.1016/j.cell.2016.09.035 (2016).
89 Brick, K., Smagulova, F., Khil, P., Camerini-Otero, R. D. & Petukhova, G. V. Genetic recombination is directed away from functional genomic elements in mice. *Nature* **485**, 642-645, doi:10.1038/nature11089 (2012).
90 Smagulova, F. *et al.* Genome-wide analysis reveals novel molecular features of mouse recombination hotspots. *Nature* **472**, 375-378, doi:10.1038/nature09869 (2011).